Geomechanics and Engineering, *Vol. 12*, *No. 4* (*2017*) *639-655*
DOI: https://doi.org/10.12989/gae.2017.12.4.639

Analysis of the thresholds of granular mixtures using the discrete element method

Gong Jian and Liu Jun*

State Key Laboratory of Coastal and Offshore Engineering,
Dalian University of Technology, *Dalian*, *China*

(*Received July 21*, *2016*, *Revised December 01*, *2016*, *Accepted December 09*, *2016*)

Abstract. The binary mixture consists of two types of granular media with different physical attributes and sizes, which can be characterized by the percentage of large granules by weight (P) and the particle size ratio (α). Researchers determine that two thresholds (P_S and P_L) exist for the peak shear strength of binary mixtures, i.e., at $P \leq P_S$, the peak shear strength is controlled by the small granules; at $P \geq P_L$, the peak shear strength is controlled by the large granules; at $P_S \leq P \leq P_L$, the peak shear strength is governed by both the large and small granules. However, the thresholds of binary mixtures with different α values, and the explanation related to the inner details of binary mixtures to account for why these thresholds exist, require further confirmation. This paper considers the mechanical behavior of binary mixtures with DEM analysis. The thresholds of binary mixtures are found to be strongly related to their coordination numbers Z_L for all values of α, where Z_L denotes the partial coordination number only between the large particles. The arrangement structure of the large particles is examined when P approaches the thresholds, and a similar arrangement structure of large particles is formed in both 2D and 3D particle systems.

Keywords: thresholds; granular mixtures; partial coordination number; porosity; direct shear test; DEM

1. Introduction

Mixtures of cohesionless granular materials are ubiquitous in nature due to multiple mechanisms, such as sand-sand mixtures with different sizes and shapes due to sedimentation, (Shin and Santamarina 2013), crushed sandstone-mudstone mixtures after excavation because of the interbedded deposit structure (Wang *et al*. 2013), and rockfill-sand mixtures in many natural slopes and rockfill structures due to weathering and deposition (Vallejo 2001). These mixtures typically consist of two or more different types of granular media, and the use of these natural mixtures is increasing in various fields, such as embankment, road and earth-dam construction. As a result, the investigation of the shear strength characteristics of such granular mixtures is important for practical applications (Hamidi *et al*. 2012).

For a special granular material mixture, the binary mixture consists of only two types of granular media with different physical attributes and sizes. Such binary mixtures can be characterized by two parameters, the percentage of large granules by weight (P) and the particle

*Corresponding author, Professor, E-mail: junliu@dlut.edu.cn
[a] Ph.D. Student, E-mail: gjdlut@mail.dlut.edu.cn

http://www.techno-press.org/?journal=gae&subpage=7 ISSN: 2005-307X (Print), 2092-6219 (Online)

size ratio α (= D_L/D_S), where D_L and D_S denote the diameters of the large and small granular media, respectively. Ogarko and Luding (2013) suggested that any ploydispersity can be replaced by an equivalent binary mixture when the size distribution moments are matched. By summarizing the results of triaxial tests conducted by various researchers on granular binary mixtures, Vallejo (2001) found that two thresholds exist for large granular material content (i.e., P_S and P_L) of granular binary mixtures for their peak shear strength: at $P \leq P_S$, the peak shear strength of the binary mixtures was controlled by the small granules and was basically equal to that of an assembly with zero large granule; at $P \geq P_L$, the peak shear strength of the binary mixtures was controlled by the large granules and was basically equal to that of an assembly with zero small granule; and at $P_S \leq P \leq P_L$, the shear strength of the binary mixtures was equal to the partial shear strength provided by the large granules plus the partial shear strength provided by the small granules. An example of gravel and sand-size particle mixtures, which are often encountered in many natural slopes and rockfill structures, is illustrated in Fig. 1. The figure conceptually displays the contribution of the different particles to the shear strength of the mixtures with consideration of the relative concentrations of the large granules. Fig. 1 illustrates that these two thresholds are important for assessing the engineering properties of mixtures. An improved understanding of the thresholds of the binary mixtures may lead to improved designs, lower-scale tests and the ability to perform knowledge-based design decisions.

Many in situ and laboratory investigations involving the determination of the shear strength of granular binary mixtures have been conducted to date. Vallejo (2001) reported a review of shear strength measurements carried out on mixture proportions that varied between 0% and 100% of gravel and sand by various researchers. The average of the reported findings and those measured by the authors were rather consistent, i.e., when the weight concentration, P, exceeds 70%, the behavior of the mixture is governed by the large granules (i.e., P_L = 70%), and when it is less than 40%, the small granule content has the predominant role (i.e., P_S = 40%). Similar thresholds of binary granular mixtures regarding shear strength were also supported by other researchers. For example, Kuenza *et al*. (2004) investigated the undrained shear behavior of sand with gravel via torsional shear tests and found that the effect of gravel content on the strength is insignificant until the gravel content is approximately 40% (i.e., P_S = 40%). Simoni and Houlsby (2006) and Xu *et al*. (2011) explored the binary granular mixture named soil-rock through large-scale direct shear tests and observed that the thresholds are P_S = 30% and P_L = 70%, respectively.

To date, only a few studies have attempted to explain why these thresholds (i.e., P_S = 40% and P_L = 70%) exist. Based on the changes in porosity when different proportions of large and small

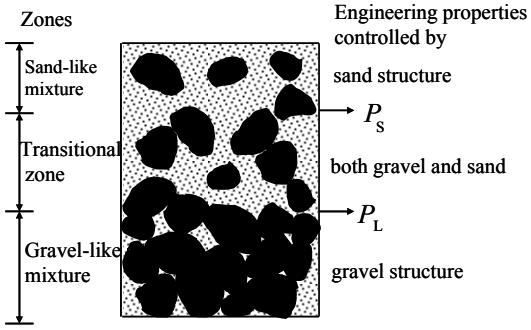

Fig. 1 Gravel-sand mixtures in many natural slopes and rockfill structures

glass beads are mixed, Vallejo (2001) presented an explanation as to why P_S is 40% and P_L is 70%. However, this explanation was mainly based on an inferred fabric in the large and small granular mixture when P approached the threshold. Therefore, further inner details of binary mixtures must be investigated to gain an understanding of the microstructure of binary mixtures when P reaches the thresholds. Fragaszy *et al*. (1992) described a matrix model regarding the thresholds (i.e., P_S and P_L) of sandy gravel, which related the state of large-large granule contact to the thresholds of binary mixtures. The large granules are in a floating state (i.e., there is little contact between large particles) when P is less than P_S, whereas the large granules begin to make contact with each other when P is larger than P_L. However, there is only a qualitative description regarding the relationship between the thresholds and the state of large-large contacts to date, and a quantitative relationship between them requires further confirmation. Alternatively, many types of binary mixture systems with different α values can be found in geotechnical engineering, such as sand-sand mixtures with an α close to one (Shin and Santamarina 2013) and waste rock-fine tailings mixtures with an α that approaches one thousand (Khalili 2009). Previous research studies found that the behaviors of a binary mixture are also affected by α in many aspects, including packing porosity (Lade *et al*. 1998) and normal-shear stress behavior (Hassanpour *et al*. 2004). Ueda *et al*. (2011) investigated the mechanical properties of binary mixtures and presented a model to predict the thresholds of binary mixtures with different values of α. However, the thresholds obtained from this model are different from the thresholds when α = 12.5 (i.e., the α of glass beads that was used in Vallejo 2001), and the reason for this may be related to the model presented by Ueda *et al*. (2011), which is also based on an inferred fabric when P reaches the thresholds. Therefore, the relationship between the thresholds (i.e., P_S and P_L) and α also needs further confirmation.

The two-dimensional discrete element method (DEM) (Cundall and Strack 1979) is used to perform the numerical experiments in this study. One advantage to using the DEM is that many significant micro-structural quantities, including contact forces net, coordination number, and porosity, can be directly measured, but these quantities are inaccessible in physical experiments. In the past, the two-dimensional DEM has been demonstrated to be capable of generating reliable results for granular matter subject to microstructure analysis (Wang *et al*. 2014). Using the DEM, the microstructures of binary mixtures are investigated in this paper, and thresholds of binary mixtures (i.e., P_S and P_L) with different values of α are obtained. The emphasis is placed on obtaining a quantitative relationship between the thresholds and the state of large particles in contact.

2. DEM simulation

Numerical direct shear tests are conducted on binary mixtures with different values of P and α. The numerical experiments are mainly carried out using the discrete element code PFC^{2D}. In addition, the effectiveness of the results is validated using PFC^{3D}. In all tests, the diameter of small particles is 1.0 mm, and the diameters of large particles are 1.0, 2.0, 5.0 and 9.5 mm for different values of α. Fig. 2 shows the typical particle size distribution curves of binary mixtures with α = 2.0 and α = 9.5. The diameters of both large and small particles have a 12.5% deviation from their diameters to prevent particles from order configuration (Oger *et al*. 2007). The particle size distributions of binary mixtures with α = 1.0 and α = 5.0 are not plotted here because they exhibit the same trends shown in Fig. 2. The binary mixtures are prepared by mixing various proportions of large and small particles, as shown in Table 1, and the number of disks for different values of α

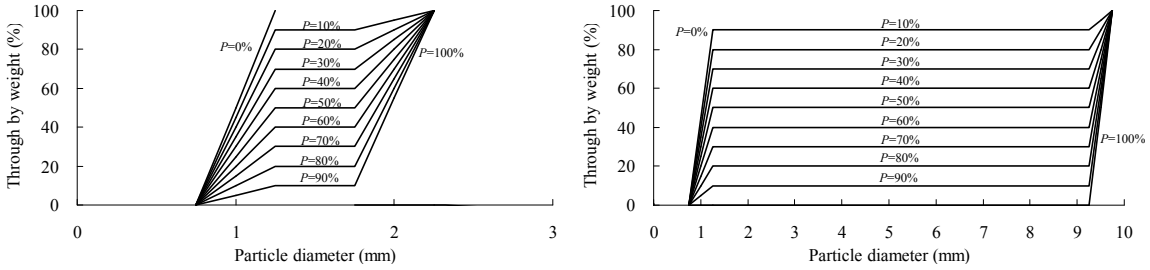

Fig. 2 The particle size distributions of binary mixtures with different α (a) $\alpha = 2$; (b) $\alpha = 9.5$

corresponding to different values of P are also summarized in Table 1. Fig. 3 shows a schematic diagram of the square shear box. To eliminate the specimen size effect, different size shear boxes are used for different particle size ratios. Jamiolkowski *et al*. (2004) suggested that the ratio of the specimen diameter to the maximum particle size (B/D_{max}) should be greater than 5, with an ideal ratio of 8, to minimize stress non-uniformities arising from large particles inside a test specimen. The size of the shear box for different values of α and the ratio of the shear box size to the maximum diameter of large particles are summarized in Table 1. The shear box is composed of eight rigid frictionless boundaries, as shown in Fig. 3, and two additional flanges (i.e., walls 7 and 8) are added to prevent particle leakage during shear.

The assemblies of granular mixtures are subjected to DEM analyses in the following steps. (1) The large and small disks are generated above the shear box randomly under the conditions of the given P and α values. The generated disks then fall down freely under gravity without friction to form a dense assemblage. Frictionless conditions can form densest assemblies for a given generation procedure, so the assemblies with different P are at the same relatively density. (2)

Table 1 Summary of sample size and total number of particles for different DEM materials

		Binary mixtures			
		$\alpha = 1.0$	$\alpha = 2.0$	$\alpha = 5.0$	$\alpha = 9.5$
Box size, $B \times B$ (mm)		50×50	100×100	125×125	250×250
B/D_{max}		44	44	22	23
Total number of particles	$P = 0\%$	2773	11180	18080	73515
	$P = 10\%$	2772	10373	16006	64019
	$P = 20\%$	2770	9529	14455	57228
	$P = 30\%$	2776	9159	12661	51117
	$P = 40\%$	2777	8490	11251	44562
	$P = 50\%$	2773	7796	9511	37940
	$P = 60\%$	2771	7126	7817	30679
	$P = 70\%$	2768	6413	6036	23350
	$P = 80\%$	2740	5734	4348	16165
	$P = 90\%$	2776	5001	2452	8387
	$P = 100\%$	2768	4331	678	761

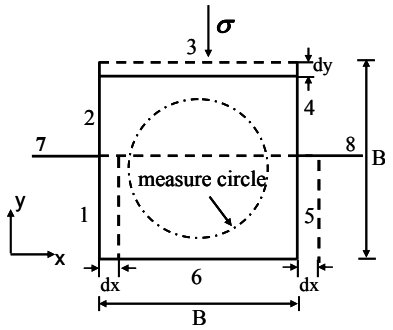

Fig. 3 The schematic diagram of the direct shear box

Granular assemblies are compressed by moving the top wall (i.e., wall 3 as shown in Fig. 3) through an iterative and controllable mechanism until the target pressure (100 kPa) is reached. (3) The porosity and coordination number are measured after the equilibrium process is stabilized. (4) The inter-particle friction coefficient is reset to the predefined value to obtain the thresholds with different values of α, and then, numerical direct shear tests are carried out. The assemblies are sheared by moving the low shear box horizontally at a speed of 0.005 m/s (also used in Gong and Liu 2015) under the application of constant vertical stress acting on the top wall. The shear resistance and deformation of the assemblies are monitored during the shear process. The shear resistance is obtained by dividing the horizontal reaction force of the lower half of the box by the shear area of the shear box (Zhang and Thornton 2007).

3. Simulation results

3.1 Approximate extent of the threshold

The shear strength of a granular mixture is provided by the contact of its particles. There are three types of contact for binary mixtures, large-large particle (LL) contact, large-small particle (LS) contact and small-small particle (SS) contact, which depend on the two entities being in contact. The friction effect of the particle contact on the shear strength of the granular mixture can be determined by changing the friction coefficient of particles. By changing the friction coefficient of different contact types, the contribution of each type of contact on the shear strength of the binary mixture can be evaluated. This method allows for the determination of which contact type has the dominant effect on the shear strength of the binary mixtures and, in some cases, which type

Table 2 The friction coefficient of the simulation cases in DEM analysis

Case	Large particles (f)	Small particles (f)	LL contacts (f_{LL})	LS contacts (f_{Ls})	SS contacts (f_{ss})
1	0.5	1.0	0.5	0.5	1.0
2	1.0	1.0	1.0	1.0	1.0
3	1.0	0.5	1.0	0.5	0.5
4	0.5	0.5	0.5	0.5	0.5

Table 3 Input parameter of analysis

Porperty	Density (kg/m^3)	Damping contant	Normal stiffness k_n (kN/m)	Shear stiffness k_s (kN/m)	Friction coefficient f
Particles	2650	0.7	1.5e7	1.5e7	as shown in Table 2
Walls	-	-	1.3e9	1.3e9	0

of contact's contribution is negligible. Based on this idea, four cases are designed and listed in Table 2, which means that each assemblage is sheared four times. By comparing cases 1 and 2, one can obtain the approximate bound of P_S and the approximate bound of P_L based on the results from cases 3 and 4.

The linear contact model is used in DEM analysis, and the parameters are presented in Table 3.

The results for the peak angle of shear resistance of the binary mixtures for different values of P and α are listed in Table 4.

For a specific α, changes in P will result in changes in the peak friction angle of the binary mixtures even if all particles have the same friction coefficient (i.e., cases 2 and 4 for various values of α, as listed in Table 4). This effect arises from the geometric factors of the binary granular system, such as the roller effect (Saowapark *et al*. 2009) and solid inclusion effect (Simoni and Houlsby 2006). However, the difference between cases 2 and 1 indicates the contribution from the *LS* and *LL* contact to the peak friction angle of the shear resistance, without

Table 4 The peak angle of shear resistance of binary mixtures with different P and α

α	Case	ϕ_{max} (deg)										
		P = 0%	P = 10%	P = 20%	P = 30%	P = 40%	P = 50%	P = 60%	P = 70%	P = 80%	P = 90%	P = 100%
1.0	1	35.4	34.5	36.0	32.7	30.6	30.1	32.2	30.4	28.4	34.1	29.1
	2	35.4	34.5	36.0	36.1	34.6	33.9	38.7	37.1	33.8	39.3	35.5
	3	28.9	28.8	29.7	31.0	28.6	31.9	35.3	35.0	31.9	36.4	35.4
	4	28.9	28.8	29.7	31.0	28.6	30.2	32.2	31.6	27.5	31.9	29.1
2.0	1	35.2	32.4	31.7	32.9	32.1	32.0	29.7	29.9	31.0	29.7	30.7
	2	35.2	32.4	32.4	32.9	35.0	36.1	33.8	35.5	35.4	35.8	36.9
	3	28.8	27.2	29.5	26.8	30.1	29.6	29.9	31.4	33.8	34.0	36.1
	4	28.8	27.2	29.5	26.8	30.1	29.6	28.2	29.6	31.5	30.0	30.9
5.0	1	35.4	33.8	34.4	32.9	34.3	34.1	34.1	35.3	33.0	36.0	44.7
	2	35.4	33.8	34.4	32.9	35.3	37.0	35.1	37.7	36.8	33.4	40.0
	3	28.9	28.8	28.8	27.9	28.8	30.4	29.3	34.1	33.2	36.6	44.7
	4	28.9	28.8	28.8	27.9	28.8	30.4	29.3	33.0	31.4	34.6	40.2
9.5	1	35.1	32.2	31.4	31.4	32.4	33.8	32.7	27.7	34.8	36.7	37.1
	2	35.1	32.2	31.4	31.4	32.4	35.6	35.9	37.3	39.3	39.0	42.0
	3	28.8	27.9	25.6	27.7	27.0	27.9	29.2	33.0	35.0	38.0	42.0
	4	28.8	27.9	25.6	27.7	27.0	27.9	29.2	31.4	32.2	35.0	36.9

regard to the effects of geometric factors. Fig. 4 plots the differences against the large particle content, P. Alternately, the difference between cases 3 and 4 represents only the effects of LL contact on the peak angle of the shear resistance, and this is plotted in Fig. 5. The vertical axes in Figs. 4-5, ϕ_{PS} and ϕ_{PL}, are the differences in the peak friction angle of the shear resistance and are defined as follows

$$\phi_{PS} = \phi^{2}_{\max} - \phi^{1}_{\max} \tag{1}$$

$$\phi_{PL} = \phi^{3}_{\max} - \phi^{4}_{\max} \tag{2}$$

where $\phi^{1}_{\max}$, $\phi^{2}_{\max}$, $\phi^{3}_{\max}$ and $\phi^{4}_{\max}$ are the peak friction angles of the shear resistance of the binary mixtures when the friction coefficients of the particles are set to the values corresponding to cases 1-4, as listed in Table 2. Based on the aforementioned definitions of P_S and P_L, when $P \le P_S$, SS contact plays the primary role in the shear response of binary mixtures, whereas the contribution from LL and LS contact is negligible. This indicates that ϕ_{PS} will be close to zero when $P \le P_S$. Alternately, when $P \ge P_L$, LL contact begins to play a greater role in the shear response of the binary mixtures, whereas LS and SS contact begin to disperse and provide a secondary effect, which indicates that ϕ_{PL} will be close to zero when $P < P_L$.

Figs. 4-5 illustrate that it is difficult to obtain precise values for P_S and P_L because only some discrete cases with different P values are conducted. However, the approximate ranges of P_S and P_L can be determined for a binary mixture with a specific α. For example, the ϕ_{PS} curve for $\alpha = 2$ in Fig. 4 indicates that the P_S of binary mixtures with $\alpha = 2$ should be within the range of 30% and 40%. The ϕ_{PL} curve for $\alpha = 5$ in Fig. 5 indicates that the P_L of binary mixtures with $\alpha = 5$ should be within the range of 60% and 70%.

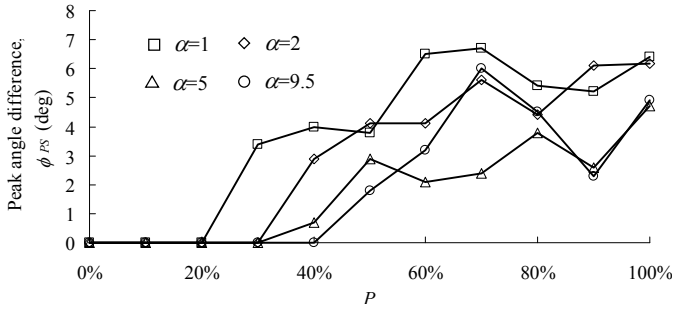

Fig. 4 The relationship between peak angle difference ϕ_{PS} and the content of large particles P

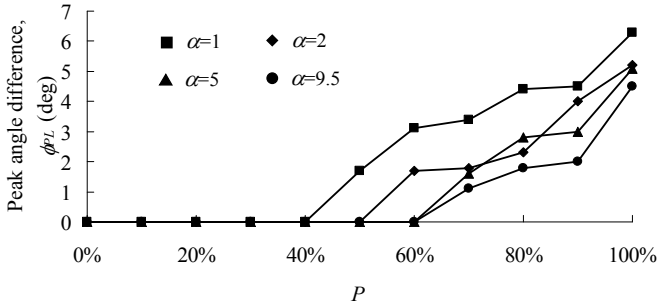

Fig. 5 The relationship between peak angle difference ϕ_{PL} and content of large particles P

Table 5 the approximate ranges of P_S and P_L which are obtained from Figs. 4-5

Thresholds	α			
	1.0	2.0	5.0	9.5
P_S	$20\% \le P_S < 30\%$	$30\% \le P_S < 40\%$	$30\% \le P_S < 40\%$	$40\% \le P_S < 50\%$
P_L	$40\% \le P_L < 50\%$	$50\% \le P_L < 60\%$	$60\% \le P_L < 70\%$	$60\% \le P_L < 70\%$

Table 5 summarizes the ranges of P_S and P_L obtained from the analysis of Figs. 4-5. The precise thresholds require further confirmation based on the turning points of the structural characteristics (i.e., porosity and partial coordination number) when P approaches the thresholds.

3.2 Thresholds determined by the porosity and partial coordination number

3.2.1 Porosity

A parameter P_{Lm} can be defined as the corresponding P when a binary mixture develops its minimum porosity. Vallejo (2001) concluded that P_{Lm} can be regarded as P_L through a series of direct shear tests on binary glass beads. The relationships between porosity, n, and P with different values of α are examined, as shown in Fig. 6. The porosity in the measure circle shown in Fig. 3 was measured after the normal pressure was applied. The porosity is defined by $n = V_v/V$, where V_v is the total area of porosity in the measure circle and V is the area of the measure circle. To prevent the 'wall effect' from influencing the porosity measurement, the measure circle is four times the diameter of the large particle away from the wall, as shown in Fig. 3. From Fig. 6, the porosity of the sample composed of mono-size particles ($\alpha = 1$) is observed to be nearly constant, as expected. However, the variation of porosity n with P shows a 'U' shape for other binary mixtures. The same tendency was observed in many experiments conducted by various researchers (e.g., Garga and Mdreira 1985, Vallejo 2001 and Lade *et al*. 1998).

At the beginning with 0% large particles, the small particles form a structure with an initial porosity. Large particles are then put into the primary fabrics of small particles. The large particles are considered to float in the matrix of small particles at the time. In fact, it can be considered that the volumes of small particles and a portion of porosity are replaced by the volumes of the floating large particles when the large particle content increases. The sample porosity thus gradually decreases with an increase in the large particle content P. Decreasing in porosity continues until the skeleton of large particles form in the sample. At that time, most of the small particles are

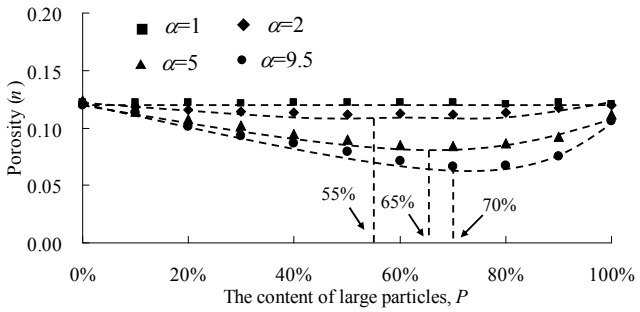

Fig. 6 The relationship between porosity of binary mixtures and P with different α

confined in the skeleton voids of large particles. A further increase in the large particles and decrease in the small particles will result in the increase in skeleton voids of large particles. Thus, the sample porosity increases with a further increase in P. Therefore, the porosity of mixtures exhibits a "U" shape with the increase of P value as indicated in Fig. 6.

The approximate P_{Lm} of the binary mixtures with different values of α (except for $\alpha = 1$) are shown in Fig. 6. Because the porosity is the same for mono-size mixtures (i.e., $\alpha = 1$) with different values of P, the value of P_{Lm} of a binary mixture with $\alpha = 1$ cannot be estimated. As noted above, the constant P_L approaches 70% for many natural binary mixtures. This implies that the porosity of binary mixtures is typically developed to their minimum value when P approaches 70%, and this phenomenon is observed in many experiments (e.g., Garga and Mdreira 1985, Shelley and Daniel 1993 and Vallejo 2001). However, Fig. 6 illustrates that the phenomenon of P_{Lm} approaching 70% is only observed in cases of binary mixtures with $\alpha = 9.5$. For other binary mixtures, P_{Lm} is found to be less than 70%. P_{Lm} is observed to increase as α increases, which agrees with previous experimental studies (e.g., Mota *et al*. 2001, Zhang *et al*. 2011). Furthermore, Yu and Standish (1987) reanalyzed a considerable amount of experimental data from other published works and proposed the following relation between P_{Lm} and α

$$P_{Lm} = (1 - 1/\alpha^2)/(1 + n_0) \times 100\% \tag{3}$$

where n_0 represents the porosity of the pure large or small granular assemblage. Fig. 7 shows the porosity of random mono-size particle packings, the data of which are extracted from different literatures for round materials, such as glass beads (i.e., Yerazunis *et al*. 1962, Mota *et al*. 2001 and Zhang *et al*. 2011) and steel balls (i.e., Mcgeary 1961 and Pinson *et al*. 1998).

From Fig. 7, it can be observed that the porosity varies over a small range irrespective of the particle size. By substituting the average of the reported values in Fig. 7 ($n_0 = 0.39$) into Eq. (3), P_{Lm} can be written as

$$P_{Lm} = 0.719(1 - 1/\alpha^2) \times 100\% \tag{4}$$

Eq. (4) illustrates that P_{Lm} will increase gradually with increasing α and that P_{Lm} will increase to a plateau value of approximately 72% as α increases to a large value. $P_{Lm} = 72\%$ also supports the conclusion of Vallejo (2001) that P_{Lm} can be regarded as P_L (i.e., constant $P_L = 70\%$) for many natural binary mixtures with a sufficiently large α. By substituting $\alpha = 1$ into Eq. (4), we can

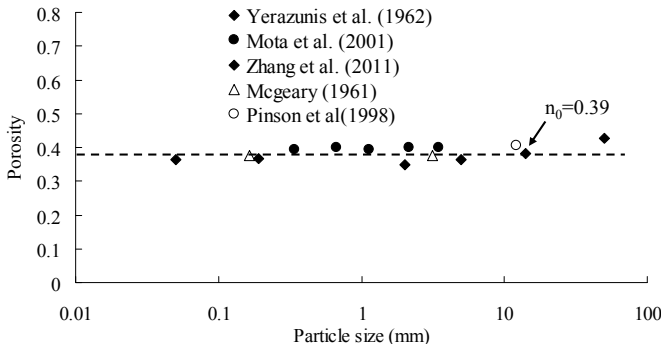

Fig. 7 The relationship between the porosity of the round material against the particle size

obtain the result of P_{Lm} = 0%. P_{Lm} = 0% contradicts the conclusion of Vallejo (2001) because the shear behavior of binary mixtures cannot be controlled by the large particles when P = 0 even though the two components have the same size. Nearly all of the α values reanalyzed in the report of Yu and Standish (1987) are greater than 2, in this case, the P_{Lm} value predicted by Eq. (4) for $1 \le \alpha < 2$ should be reevaluated. As stated by Fragaszy *et al*. (1992), the thresholds of binary mixtures are related to the state of large particles in contact. Therefore, the relationship between the porosity and partial coordination number of large particles is examined in the following paragraphs, aiming at evaluating the P_{Lm} of a binary mixture when $1 \le \alpha < 2$ and then obtaining precise thresholds of binary mixtures with different values of α.

3.2.2 Partial coordination number

The mean partial coordination number Z_L is defined as the total number of contacts between the large particles C_L divided by the total number of large particles N_L (i.e., $Z_L = 2C_L/N_L$). Z_L is measured after the normal pressure was applied and before shear. Fig. 8 shows Z_L for binary mixtures with various values of α with respect to the content of large particles, P. Fig. 8 illustrates that Z_L increases gradually with increasing P, which also can be observed in the report of Pinson *et al*. (1998). The Z_L curve varies linearly with increasing P for binary mixtures with α = 1. However, for other binary mixtures, the evolution of Z_L is observed to be related in a non-linear manner with respect to P, and the curvature appears to increase gradually with increasing α when $\alpha < 5$. In addition, for Z_L curves of binary mixtures with α = 5.0 and α = 9.5, locations from the two curves

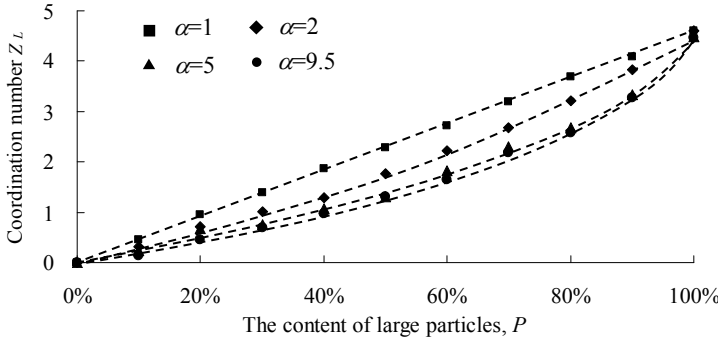

Fig. 8 Z_L for binary mixtures with various values of α with respect to P

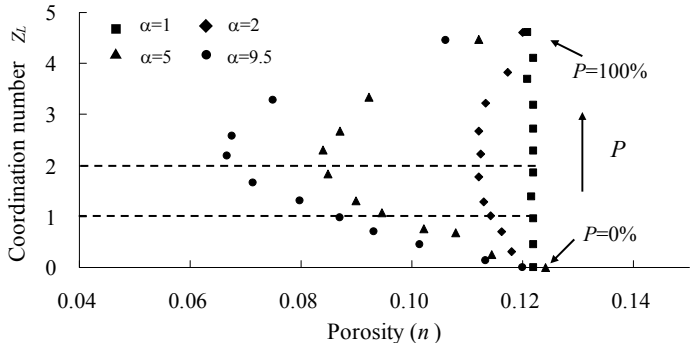

Fig. 9 The evolution of Z_L as a function of porosity for various P and α.

Table 6 The P_{Lm} for binary mixtures with different α

Parameters	α			
	1.0	2.0	5.0	9.5
P_{Lm} (Z_L = 2 in Fig. 9)	41%	55%	64%	68%
P_{Lm} (using Eq. (4))	0%	54%	68.5%	70.6%
P_{Sm} (Z_L = 1 in Fig. 9)	21%	30%	39%	40%

are close to each other, which suggests that the evolution of Z_L with respect to P is less sensitive to α when $\alpha \geq 5.0$. The small particles can occupy the smallest voids in the densest possible packing of large particles when $\alpha \geq 6.48$ (Lade *et al*. 1998). In other words, small particles occupy the voids within a dense packing of large particles without greatly disrupting its skeleton when $\alpha \geq 6.48$. The particle size ratio $\alpha = 5.0$ is close to $\alpha = 6.48$, which may be an explanation why the evolution of Z_L with respect to P is sensitive to α when $\alpha \geq 5.0$ as indicated in Fig. 8.

Fig. 9 shows the evolution of Z_L with respect to porosity for binary mixtures with different values of P and α. The porosities of all binary mixtures develop their minimum values when Z_L = 2.

Table 6 summarizes the P_{Lm} for binary mixtures with different values of α, which can be obtained by linear interpolation of the two adjacent points when Z_L = 2 in Fig. 9, and the calculated P_{Lm} (i.e., using Eq. (4)) of binary mixtures with different α values are also included.

In Table 6, although the presented work is developed in a 2D particle system, the values of P_{Lm} obtained by Z_L = 2 are close to the calculated P_{Lm} determined by a 3D particle system, except for the binary mixture with $\alpha = 1$. This observation implies that there exists a similar geometrical structure when P approaches the P_{Lm} in both the 2D and 3D particle systems, which will be analyzed in a later section. Comparing the P_{Lm} (corresponding to Z_L = 2) in Table 6 with the range of P_L shown in Table 5, the value of P_{Lm} is located in the range of P_L. The result suggests that the values of P_{Lm} can be regarded as P_L for binary mixtures with different values of α, which is consistent with the conclusion of Vallejo (2001). Additionally, as shown in Fig. 8, the Z_L curves are less sensitive to α when $\alpha \geq 5$. This observation suggests that P_L will also be less sensitive to α when $\alpha \geq 5$, as P_L can be directly obtained from the P of the binary mixture corresponding to Z_L = 2. Considering that the values of α of most binary mixtures in geotechnical engineering are conventionally larger than 5, P_L is believed to be a constant value (i.e., approaching 70%). Assuming that the P_L limit of a binary mixture is 70% when α goes to infinity and combining the data of P_{Lm} obtained from Z_L = 2 in Table 6, the relationship between P_L and α can be fitted with the following equation

$$P_L = (0.70 - 0.292/\alpha^{1.007}) \times 100\% \tag{5}$$

Compared to Eq. (4), Eq. (5) indicates a modified expression that can also be applied for binary mixtures with $1 \leq \alpha < 2$ to obtain P_L.

According to the matrix model described by Fragaszy *et al*. (1992), the thresholds of binary granular mixtures are related to the state of *LL* contact. It has previously been confirmed that Z_L = 2 corresponds to the P of binary mixtures that can be regarded as P_L. Thus, there likely also exists a $Z_L = k_0$ corresponding to the P of binary mixtures, and this P can be regarded as P_S, where k_0 is a specific constant and less than 2 for binary mixtures with different values of α. As shown in Table

6, the threshold P_L = 68% for α = 9.5 is observed to be close to the P_L = 70% conducted by Vallejo (2001) for binary glass beads with α = 12.5. Therefore, the P_S for α = 9.5 is also close to the P_S = 40% conducted by Vallejo (2001). Fig. 9 shows that Z_L is 1 when P approaches 40% for binary mixtures with α = 9.5. Thus, k_0 = 1. A parameter P_{Sm} is defined as the corresponding P when the binary mixtures reach Z_L = 1, and Table 6 summarizes the P_{Sm} for binary mixtures with different values of α, which can be obtained by linear interpolation of the two adjacent points when Z_L = 1 in Fig. 9. Comparing P_{Sm} in Table 6 to the range of P_S shown in Table 5, the values of P_{Sm} are located in the range of P_S. This result suggests that the P_{Sm} of binary mixtures can be regarded as P_S. In other words, as the P of a binary mixture increases until Z_L = 1, the role of large particles on the peak shear strength of binary mixtures cannot be negligible. The limit P_S is believed to be 40% for binary mixtures with sufficiently large values of α (Vallejo 2001 and Kuenza *et al*. 2004), and then, combining the data of P_S shown in Table 6, the relationship between P_S and α can be fitted by the following equation

$$P_S = (0.40 - 0.195/\alpha^{1.242}) \times 100\% \tag{6}$$

Fig. 10 plots the thresholds of granular mixtures against the particle size ratio α based on the Eqs. (5) and (6). At the beginning with P_S = 20.5% and P_L = 40.8% for α = 1.0, P_S and P_L then gradually increase with α and approach 40% and 70% respectively when α is sufficiently large.

3.3 Relationship between the thresholds and arrangement structure of large particles

Fig. 11 shows the configuration of granular assemblies with α = 5.0 under different levels of P. The figure is used to gain an understanding of the particle packing and microstructure characteristics acquired by binary mixtures, which includes six diagrams of packing structures corresponding to states a through f. In particular, states c and d are defined by P = 40% and P = 70%, which can be regarded as the states at which P reaches the thresholds P_S and P_L, respectively.

It has previously been concluded that the minimum porosity of binary mixtures corresponding to P can be regarded as the P_L for various values of α. The minimum porosity of binary mixtures is often a concern in various fields, and many publications (e.g., Vallejo 2001, Zhang *et al*. 2011 and

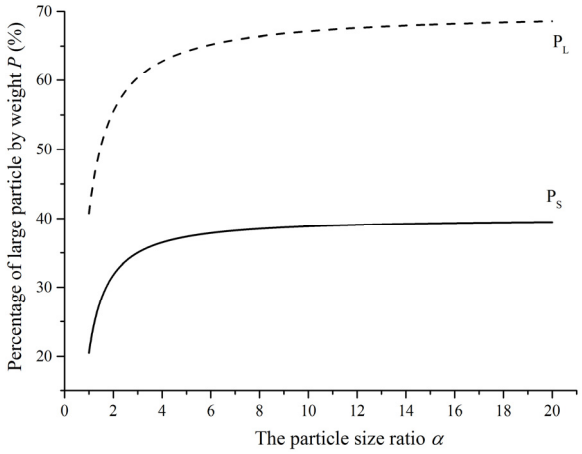

Fig. 10 The evolution of P_S and P_L with α based on Eqs. (5) and (6)

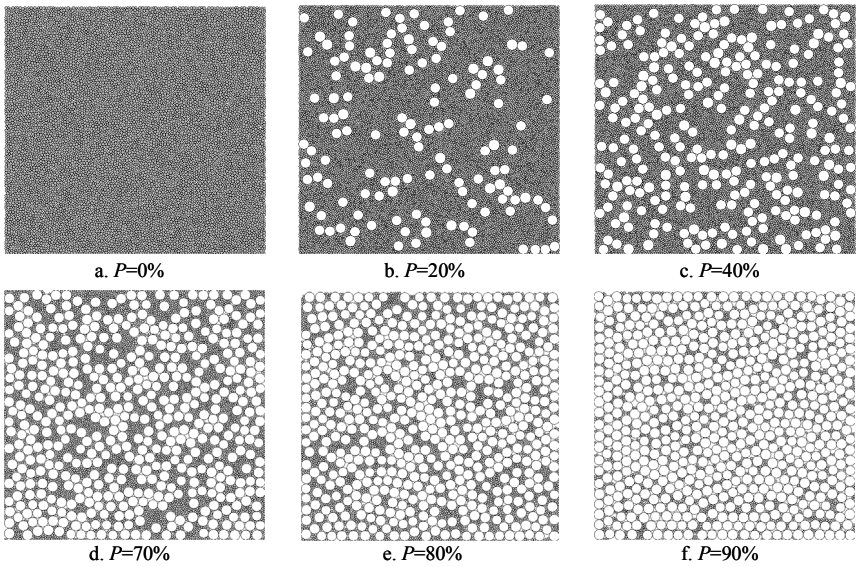

Fig. 11 An assembly with $\alpha = 5$ under different levels of P after normal pressure was applied

Ueda *et al*. 2011) consider this minimum porosity as theoretically occurring when small particles completely fill the voids of the load-bearing large particles, and the schematic structure is plotted in Fig. 12a. However, Fig. 11 illustrates that the structure shown in Fig. 12(a) does not appear to be the case even though $P \geq P_L$. The theoretical condition can only emerge when α is sufficiently large (Lade *et al*. 1998), otherwise, the small particles tend to wedge into the skeleton of large particles, as illustrated in Fig. 12(b). Based on the geometrical structure when the porosities of binary mixtures develop their minimum value, as shown in Fig. 12(a), Vallejo (2011) found that the predicted porosity is smaller than the actual value. The reason for this is related to the wedging effects, which will result in an increased porosity compared to the theoretical structure shown in Fig. 12(a). Therefore, understanding the actual structure of binary mixtures when P approaches the thresholds is important, as an inferred fabric mixture may lead to error when predicting the state of binary mixtures.

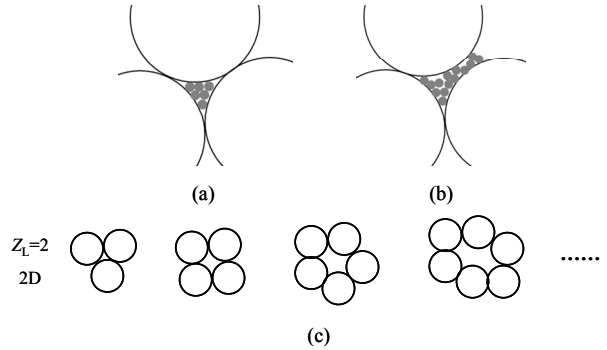

Fig. 12 Schematic representation of the arrangement of particles: (a) small particles fill the free space between large particles; (b) small particles wedge in the skeleton of large particles; (c) the hollow and circle structure formed by enclosing the large particles

The results of numerical direct shear tests confirm that $Z_L = 2$ corresponds to the P that can be regarded as P_L. Thus, a specific structure is thought to exist for $Z_L = 2$ for binary mixtures with different α values, which is considered helpful for understanding the behavior of binary mixtures at their turning points. From a geometrical consideration of the arrangement of large particles when $Z_L = 2$, a hollow and circular structure composed of large particles is expected to exist, which is illustrated in Fig. 12(c). The theoretical structure shown in Fig. 12(a) actually indicates a particular case of this structure. Figs. 11(d)-(f) illustrates that small particles are gradually confined in the central voids of this structure with increasing P. This indicates that the structure shown in Fig. 12(c) appears to be the case when $P \geq P_L$. If this specific structure also exists in the case of a 3D configuration, then Z_L is believed to be 3 when the porosities of binary mixtures with sufficiently large values of α develop their minimum value. If the α value of binary mixtures is not sufficiently large, the wedging effects will lead to the formation of a hollow and spherical structure enclosed by large particles, for which Z_L is also believed to be 3. To verify that the specific structure is also the case in a 3D particle system, another series of binary mixtures with P ranging from 0% to 100% was prepared for $\alpha = 1.0$, $\alpha = 1.4$, and $\alpha = 2.0$ using the discrete element code PFC^{3D}. The particle properties include the "contact Young modulus" (i.e., E_c = 1e7 Pa), which determines the stiffnesses of particles by $k_n = 4\ E_c\ R$ (R denotes the minimum radius of the two particles in contact); the ratio of the particle stiffnesses (i.e., $k_n/k_s = 1.0$); and the friction coefficients of the particles, which are set to zero to form a dense assemblage. The particle size distributions of these binary mixtures have the same trend as in Fig. 2, and the assemblies are prepared in the same process as previously mentioned. After the equilibrium process is stabilized for the generated particles that fall down freely under gravity, the Z_L of each assemble are measured, and the results are plotted in Fig. 13. The results are consistent with previous simulations (Pinson *et al*. 1998 and Biazzo *et al*. 2009) for $\alpha = 1.4$ (Fig. 13(a)) and $\alpha = 2$ (Fig. 13(b)).

After the normal pressure is applied ($\sigma = 100$ kPa), the Z_L of each assembly are measured again, and the results are plotted in Fig. 14. We can obtain the P corresponding to $Z_L = 3$ from the figure using a linear interpolation of the two adjacent points. The data are summarized in Table 7, and the calculated values of P_L (i.e., using Eq. (5)) are also included for comparison. In Table 7, it can be observed that, though Eq. (5) is developed in a 2D particle system, the calculated values of P_L are close to the P corresponding to $Z_L = 3$ in the 3D particle system. Moreover, the theoretical coordination number of frictionless mono-size spherical assembles are expected to be 4 and 6 in 2D and 3D particle systems, respectively (Roux 2000). The ratio of the coordination number in

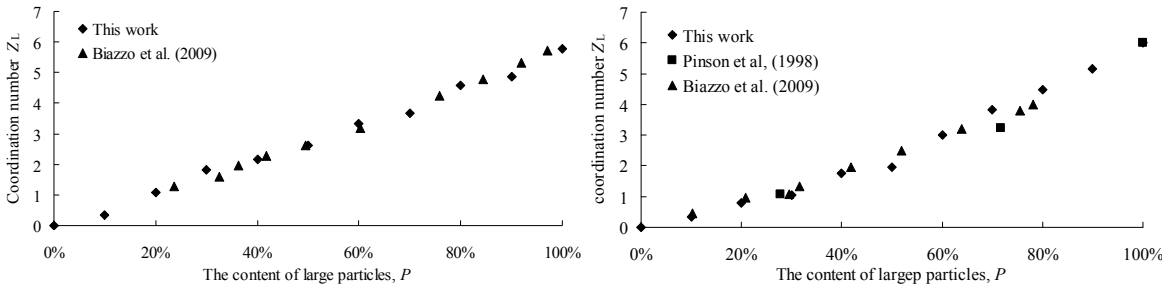

Fig. 13 Particle coordination number Z_L versus P for: (a) $\alpha = 1.4$; and (b) $\alpha = 2$

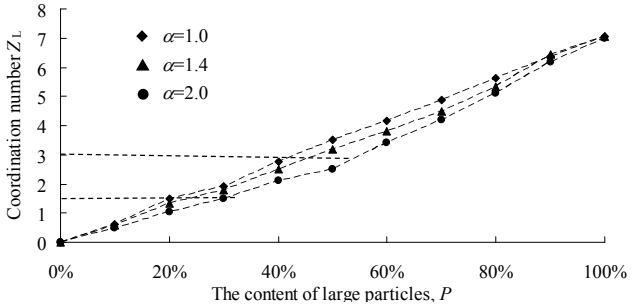

Fig. 14 The relationship between the mean partial coordination number Z_L and P in 3D particle system

Table 7 Comparison of the P between the measured value and predicted value in 3D model

α	P determined by (i.e., P_L)		P determined by (i.e., P_S)	
	Z_L = 3 in Fig. 13	using Eq. (5)	Z_L = 1.5 in Fig. 13	using Eq. (6)
1.0	41%	41%	20%	21%
1.4	45%	49%	25%	27%
2.0	53%	55%	31%	32%

a 3D mono-size particle system to that in a 2D mono-size particle system (i.e., 6/4) is the same as the ratio of Z_L in these two spatial dimensions when the porosities of binary mixtures develop their minimum value (i.e., 3/2). The results suggest that a similar arrangement structure of large particles is formed in both 2D and 3D particle systems when the porosities of binary mixtures develop their minimum value. Thus, the large particles begin to control the shear behavior of binary mixtures as Z_L reaches 3 in 3D particle systems. Moreover, Fig. 14 illustrates that the Z_L curve varies linearly when increasing P for mono-size assembles (α = 1). Then, Z_L = 1.5, corresponding to the P, can be regarded as P_S in 3D particle systems because P_L is twice the value of P_S in 2D binary mixtures with α = 1. From Fig. 14, one can obtain the P corresponding to Z_L = 1.5 by linear interpolation, which is also summarized in Table 7, and the calculated values of P_S (i.e., using Eq. (6)) are also included for comparison. In Table 7, the calculated values of P_S are also close to the P values obtained corresponding to Z_L = 1.5 in the 3D particle system.

4. Conclusions

This paper describes a 2D DEM analysis carried out to estimate the thresholds of cohesionless granular binary mixtures with different particle size ratios (α). A series of dense particle assemblies were prepared, and their porosity and mean partial coordination number Z_L were measured. To obtain the thresholds of binary mixtures, the inter-particle friction coefficients of the assemblies were reset to the different predefined values, and then, numerical direct tests were conducted. The following concluding remarks can be made:

(1) The evolution of the Z_L of binary mixtures is related with α: Z_L varies linearly with P when α = 1, and for other binary mixtures, the Z_L curves are observed to be related in a non-linear manner with increasing P. Moreover, for Z_L curves of binary mixtures with α = 5

and $\alpha = 9.5$, locations from the two curves are highly similar to each other, which suggests that the evolution of Z_L is less sensitive to α when $\alpha \geq 5$. The variation of the porosity, n, with P exhibits a 'U' shape, and Z_L is 2 for all binary mixtures with different values of α when binary mixtures develop their minimum porosity.

(2) The thresholds (i.e., P_S and P_L) of binary mixtures with different α values are obtained through numerical direct shear tests. The thresholds of binary mixtures are strongly related to their partial coordination number Z_L: $Z_L = 1$ and $Z_L = 2$ correspond to the P values that can be regarded as P_S and P_L, respectively.

(3) From a geometrical consideration of the arrangement of particles when $Z_L = 2$, a hollow and circular structure composed of large particles is expected to exist. Figs. 11(d)-(f) illustrates that the structure appears to exist when the porosities of binary mixtures develop their minimum value. Another series of binary mixtures with different values of α are conducted on a 3D particle system to verify that the specific structure is also the case in 3D models. The calculated P obtained by the 2D empirical equation is consistent with the inferred Z_L corresponding to P in the 3D model because a similar arrangement structure of large particles is formed in both the 2D and 3D particle systems when P approaches the thresholds.

Acknowledgments

This research was supported by the National Natural Science Foundation of China (51479027, 51539008).

References

Biazzo, I., Caltagirone, F., Parisi, G. and Zamponi, F. (2009), "Theory of amorphous packings of binary mixtures of hard spheres", *Phys. Rev. Lett.*, **102**(19), 195701.

Cundall, P.A. and Strack, O.D.L. (1979), "A discrete numerical model for granular assemblies", *Géotechnique*, **29**(1), 47-65.

Fragaszy, R., Su, J., Siddiqi, F. and Ho, C. (1992), "Modeling strength of sandy gravel", *J. Geotech. Eng.-ASCE*, **118**(6), 920-935.

Garga, V.K. and Mdreira, C.J. (1985), "Compaction characteristics of river terrace gravel", *J. Geotech. Eng.-ASCE*, **111**(8), 987-1007.

Gong, J. and Liu, J. (2015), "Analysis on the mechanical behaviors of soil-rock mixtures using discrete element method", *Procedia Eng.*, **102**, 1783-1792.

Hamidi, A., Azini, E. and Masoudi, B. (2012), "Impact of gradation on the shear strength-dilation behavior of well graded sand-gravel mixtures", *Sci. Iran*, **19**(3), 393-402.

Hassanpour, A., Ding, Y. and Ghadiri, M. (2004), "Shear deformation of binary mixtures of dry particulate solids", *Adv. Powder Technol.*, **15**(6), 687-697.

Jamiolkowski, M., Kongsukprasert, L. and Lo Presti, D. (2004), "Characterization of gravelly geomaterials", *Proceedings of the 5th International Geotechnical Conference*, Bangkok, Thailand, November.

Khalili, A. (2009), "Mechanical response of highly gap-graded mixtures of waste rock and tailings (paste rock)", Ph.D. Dissertation; University of British Columbia, Vancouver, Canada.

Kuenza, K., Towhata, I., Orense, R.P. and Wassan, T.H. (2004), "Undrained torsional shear tests on gravelly soils", *Landslides*, **1**(3), 185-194.

Lade, P.V., Liggio, C.D. and Yamamuro, J.A. (1998), "Effects of non-plastic fines on minimum and maximum void ratios of sand", *Geotech. Test J.*, **21**(4), 336-347.

Mcgeary, R.K. (1961), "Mechanical packing of spherical particles", *J. Am. Ceram. Soc.*, **44**(10), 513-522.

Mota, M., Teixeira, J.A., Bowen, W.R. and Yelshin, A. (2001), "Binary spherical particle mixed beds : porosity and permeability relationship measurement", *Trans. Filt. Soc.*, **4**(1), 101-106.
Ogarko, V. and Luding, S. (2012), "Equation of state and jamming density for equivalent bi- and polydisperse, smooth, hard sphere systems", *J. Chem. Phys.*, **136**(12), 124508.
Oger, L., Ippolito, I. and Vidales, A.M. (2007), "How disorder can diminish avalanche risks: effect of size distribution - Precursor of avalanches", *Granul. Matter.*, **9**(3-4), 267-278.
Pinson, D., Zou, R.P., Yu, A.B., Zulli, P. and McCarthy, M.J. (1998), "Coordination number of binary mixtures of spheres", *J. Phys. D Appl. Phys.*, **31**(4), 457-462.
Roux, J.N. (2000), "Geometric origin of mechanical properties of granular materials", *Phys. Rev. E*, **61**(6), 6802-6836.
Saowapark, T., Sombatsompop, N. and Sirisinha, C. (2009), "Viscoelastic properties of fly ash-filled natural rubber compounds: Effect of fly ash loading", *J. Appl. Polym. Sci.*, **112**(4), 2552-2558.
Shelley, T.L. and Daniel, D.E. (1993), "Effect of gravel on hydraulic conductivity of compacted soil liners", *J. Geotech. Eng.-ASCE*, **119**(1), 54-68.
Shin, H. and Santamarina, J.C. (2013), "Role of particle angularity on the mechanical behavior of granular mixtures", *J. Geotech. Geoenviron.*, **139**(2), 353-355.
Simoni, A. and Houlsby, G.T. (2006), "The direct shear strength and dilatancy of sand-gravel mixtures", *Geotech. Geol. Eng.*, **3**(24), 523-549.
Ueda, T., Matsushima, T. and Yamada, Y. (2011), "Effect of particle size ratio and volume fraction on shear strength of binary granular mixture", *Granul. Matter.*, **13**(6), 731-742.
Vallejo, L.E. (2001), "Interpretation of the limits in shear strength in binary granular mixtures", *Can. Geotech. J.*, **38**(5), 1097-1104.
Wang, J., Zhang, H., Deng, D. and Liu, M. (2013), "Effects of mudstone particle content on compaction behavior and particle crushing of a crushed sandstone-mudstone particle mixture", *Eng. Geol.*, **167**, 1-5.
Wang, Z., Ruiken, A., Jacobs, F. and Ziegler, M. (2014), "A new suggestion for determining 2D porosities in DEM studies", *Geomech. Eng., Int. J.*, **7**(6), 665-678.
Xu, W.J., Xu, Q. and Hu, R.L. (2011), "Study on the shear strength of soil-rock mixture by large scale direct shear test", *Int. J. Rock Mech. Min.*, **48**(8), 1235-1247.
Yerazunis, S., Bartoett, J.W. and Nissan, A.H. (1962), "Packing of binary mixtures of spheres and irregular particles", *Nature*, **195**, 33-35.
Yu, A.B. and Standish, N. (1987), "Porosity calculations of multi-component mixtures of spherical particles", *Powder Technol.*, **52**(3), 233-241.
Zhang, L. and Thornton, C. (2007), "A numerical examination of the direct shear test", *Geotechnique*, **57**(4), 343-354.
Zhang, Z.F., Ward, A.L. and Keller, J.M. (2011), "Determining the porosity and saturated hydraulic conductivity of binary mixtures", *Vadose Zone J.*, **10**(1), 313-321.

JS